

Melanie Kettering, Ina Grau, Nadine Pömpner, Marcus Stapf, Mieczyslaw Gajda, Ulf Teichgräber and Ingrid Hilger\*

# Means to increase the therapeutic efficiency of magnetic heating of tumors

DOI 10.1515/bmt-2015-0052

Received March 13, 2015; accepted June 26, 2015; online first September 8, 2015

**Abstract:** The treatment of tumors *via* hyperthermia has gained increased attention in the last years. Among the different modalities available so far, magnetic hyperthermia has the particular advantage of offering the possibility of depositing the heating source directly into the tumor. In this study, we summarized the present knowledge we gained on how to improve the therapeutic efficiency of magnetic hyperthermia using magnetic nanoparticles (MNPs), with particular consideration of the intratumoral infiltration of the magnetic material. We found that (1) MNPs will be mainly immobilized at the tumor area and that this aspect has to be considered when estimating the heating potential of MNPs, (2) the intratumoral distribution patterns *via* slow infiltration might well be modulated by specific MNP coating and magnetic targeting, (3) imaging of the nanoparticle depositions within the tumor might allow to correct the distribution pattern *via* multiple applications, (4) multiple therapeutic sessions are feasible because MNPs are not delivered from the tumor site during the heating process, (5) the utilization of MNPs that internalize into cells will favor the production of intracellular heating spots rather than extracellular ones, (6) utilization of MNPs functionalized with chemotherapeutic agents will allow us to exploit the additive effects of both therapeutic modalities, and (7) distinct cytopathological and histopathological alterations in target tissues are induced as a result of magnetic hyperthermia. However,

the accumulation at the tumor *via* intravenous application remains a matter of challenge.

**Keywords:** cancer; magnetic hyperthermia; magnetic nanoparticles (MNPs); nanotechnology; nanotherapy; SPION.

## Background

Hyperthermia, using a transient increase in temperature at the target region, has been considered a promising tool to treat tumors. Different heating strategies that are based upon the utilization of infrared light, radiofrequency radiation ultrasound, microwave heating, etc. have been suggested. Several strategies have been developed so far: whole-body hyperthermia deals with the application of hot air or water; *via* local hyperthermia, the tumor region is exposed to electromagnetic waves (microwaves or radiowaves). Local hyperthermia only addresses small areas, such as the tumor *per se*. Regional hyperthermia heats organs or other larger parts of the body. The first mentioned strategy is particularly applicable when single tumors in the early stages of cancers are present. Whole-body or regional hyperthermia are mainly applied when treating tumors and local or distant metastases [38].

To kill tumor cells, the dose of applied temperatures, described as the area under the temperature-time curve, is of uttermost importance: the application of temperatures between 43°C and 45°C for 60–90 min refers to hyperthermia *per se*, whereas temperatures higher than 50°C for several minutes are designated as “thermoablation” [15].

Although most of the mentioned modalities for heating of tumors utilize external heating sources that demand high efforts in appropriate focusing of the energy source in question, the application of magnetic materials right to the tumor area is expected to improve the selectivity of the treatment modality. The reason being, using internal sources, the heating doses can be deposited using minimal control and be selectively localized within the tumor area [17].

Typically, the magnetic materials are made up of an iron oxide core in the nanometer range and a coating

---

\*Corresponding author: Prof. Dr. Ingrid Hilger, Institut für Diagnostische und Interventionelle Radiologie Klinikum der Friedrich-Schiller-Universität Jena, AG Experimentelle Radiologie, Forschungszentrum Lobeda, Erlanger Allee 101, D-07747 Jena, Germany, Phone: +49-3641-9325921, Fax: +49-3641-9325922, E-mail: ingrid.hilger@med.uni-jena.de

**Melanie Kettering, Ina Grau, Nadine Pömpner, Marcus Stapf and Ulf Teichgräber:** Institute of Diagnostic and Interventional Radiology, Department of Experimental Radiology, University Hospital Jena, Erlanger Allee 101, 07747 Jena, Germany

**Mieczyslaw Gajda:** Institute of Pathology, University Hospital Jena, Ziegelmühlenweg 1, 07743 Jena, Germany

material such as chain-like polymers, surfactants, proteins, etc. [13]. Such nanoparticles (MNPs) usually exhibit a superparamagnetic behavior. During the exposure to an alternating magnetic field, the magnetization vector of the MNPs with diameters smaller than 40 nm – together with distinct magnetic field parameters – will relax according to the direction of the applied external alternating magnetic field (Neél relaxation) and/or the whole MNP will rotate (Brown relaxation) [4]. The heating capability (the so-called heating potential) of the magnetic material will strongly depend upon its structural features, such as size, shape, and microstructure, and the features of the external magnetic field [25].

Different application routes for MNPs have been considered so far. A high potential for clinical translation is associated with the intratumoral infiltration of MNPs. Hereto, particularly slow infiltration is beneficial to cope with the high interstitial pressure of the tumors. Doing so, the amounts of magnetic material can be easily controlled and it will allow the doctors to deposit rather high nanoparticle amounts. One disadvantage of this strategy is the production of mostly heterogeneous nanoparticle distribution patterns, which might lead to regions of temperature underdosage [18].

The aim of the present paper is to give an overview of ways to improve the therapeutic efficiency of magnetic hyperthermia. We will first consider the situation related to the intratumoral application and then the intravenous application of the magnetic material.

## The degree of immobilization of MNP in tumors determines heating behavior

The selection of MNPs exhibiting a sufficient heating capacity (specific absorption rate, SAR) *in vivo* is important to achieve the desired temperatures. In particular, single-core MNPs were shown to exhibit higher SAR values than the multicore MNPs of the same core size. Multicore MNPs manufactured *via* different synthesis routes showed different SAR, although they exhibited comparable core and hydrodynamic sizes. We also noted the highest SAR values for MNP suspensions in water but a strong reduction of the SAR after the immobilization of MNPs in polyvinyl alcohol (PVA) was present. Generally, MNP embedment in PVA leads to a higher immobilization of MNPs compared to agarose gels. This differential finding is the result of the polymerizing agents that the MNPs are embedded

in. They should possess pore diameters suitable for efficient immobilization of MNPs in question depending on their structural parameters. Taken together, this means that immobilization of MNPs, independent of their physicochemical properties, can distinctly affect their SAR. Similar processes are supposed to take place *in vivo*, particularly when MNPs are sticking to cells and tissues [25].

We also injected magnetic multicore MNPs into experimentally grown tumors in mice and exposed them to an alternating magnetic field ( $H=25$  kA/m,  $f=400$  kHz). The magnetic characterization of the removed tumor tissue confirmed that the particles are not able to rotate, and a temperature increase due to Brown relaxation can be nearly neglected [9]. The correct estimation of the heating potential of MNPs under “real” conditions will help in designing formulations with even better suitability for magnetic heating purposes.

## The intratumoral temperature pattern might well be influenced by the nanoparticle coating

The intratumoral infiltration of MNPs (fluidMAG; Chemcell, Berlin, Germany; clustered iron oxide particles with core diameter of 10 nm [24]) coated either with polymeric Arabic acid (ARA, carboxylic end-groups) or with polyethylene imine (PEI, amine end-groups) showed a tendency to differ in their distribution pattern after infiltration into fibrosarcoma (HT1080) tumors. The MNPs with a carboxylic end-group functionalization exhibited a rather diffuse distribution pattern, whereas the amino functionalized ones exhibited a more localized one (Figure 1A, B) as revealed *via* micro CT (mCT) imaging. The effects seem to be associated with the distribution pattern *per se* rather than the changes in the physicochemical features dependent on nanoparticle surroundings (Figure 1C–E). Accordingly, the more localized distribution patterns of the PEI-coated MNPs result in comparably higher temperatures vs. the ARA-coated ones. Therefore, the intratumoral distribution pattern might be influenced by specific nanoparticle coatings containing defined end-group functionalizations, which lead to distinct temperature distributions in tumors.

The accumulation of MNPs at the tumor area might well be increased by magnetic targeting. We could show that magnetically based cellular MNP uptake by human adenocarcinoma cells is because of suitable magnetic field gradients that intensify the temperature increase

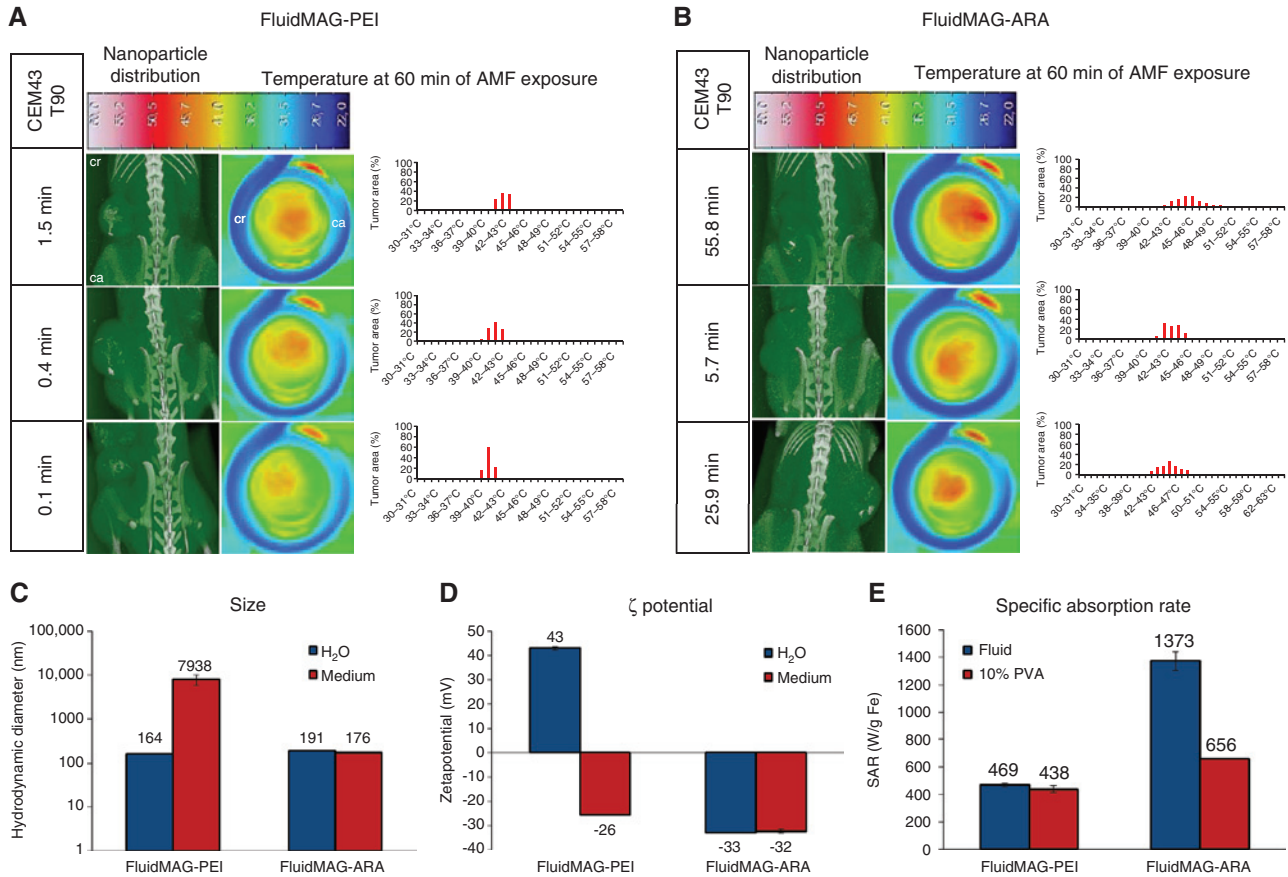


**Figure 1:** The nanoparticle end-group functionalization might influence their distribution pattern in tumors (HT1080) after slow infiltration. Intratumoral injection of 1  $\mu\text{g}$  fluidMAG-ARA (A) and fluidMAG-PEI (B) per 1  $\mu\text{l}$  tumor volume into three different mice. Cumulative equivalent minutes for 90% of the tumor volume at a temperature of 43°C; mCT images of mice to visualize MNP distribution in the tumors (dorsal view); temperature at 60 min exposure analyzed by NIRF thermal imaging (lateral view); temperature at 60 min exposure in percentage of tumor area. (C) Hydrodynamic diameter of fluidMAG-ARA and fluidMAG-PEI after 24 h incubation in dH<sub>2</sub>O and culture medium, respectively. Strong agglomeration of fluidMAG-PEI after incubation in culture medium. (D)  $\zeta$  Potential of fluidMAG-ARA and fluidMAG-PEI after 24 h incubation in dH<sub>2</sub>O and culture medium, respectively. Strong potential reversal for fluidMAG-PEI/750 after incubation in culture medium. (E) SAR of fluidMAG-ARA and fluidMAG-PEI for fluid and immobilized (in 10% PVA) MNPs. Strong loss of SAR after immobilization in 10% PVA for fluidMAG-ARA. (C–E) Mean and standard deviation of  $n=5$  (hydrodynamic diameter) and  $n=3$  ( $\zeta$  potential and SAR), respectively.

generated during magnetic heating [20]. These strategies will provide new means to avoid the occurrence of regions of temperature underdosage during magnetic hyperthermia.

## Imaging of nanoparticle depositions in tumors

Alternatively to mCT imaging, magnetorelaxometry may be an appealing system to non-invasively quantify and identify nanoparticle accumulation in tumors. Magnetorelaxometry (MRX) measurements using a multichannel vector magnetometer system with 304 superconductive

quantum interference devices allow the reconstruction of the position and magnitude of the magnetic moment from measured spatial magnetic field distributions by a magnetic dipole model fit applying a Levenberg-Marquadt algorithm. Therewith, the center of gravity and the total amount of MNP accumulation could be assessed [10].

Researchers have suggested the utilization of magnetic resonance imaging (MRI) for delineation of iron oxide deposits in tumors (e.g. [5]). Nevertheless, and apart from the occurrence of susceptibility artifacts at the tumor region *via* MRI that results from the use of high amounts of iron to obtain the appropriate local temperatures, MRI and magnetic hyperthermia are based on different and even counteracting parameters, which makes it challenging to combine them. This means that despite the versatility

of MNPs, a combination of multiple modalities (e.g. targeting, diagnostics, therapy) to one carrier has distinct limitations [16]. Appropriate imaging of local nanoparticle distributions at the tumor area (e.g. *via* X-ray, CT imaging) will allow the doctors to correct the distribution pattern *via* additional nanoparticle applications.

## MNP exposure to an alternating magnetic field does not release MNPs from the tumor

In past investigations, we showed that exposure to an alternating magnetic field does lead to a delivery of MNPs from the tumor site to other organs such as the liver and spleen. In particular, intratumoral deposition allowed for MNPs to remain stuck at the tumor at least for 7 days. At this time point, a few MNPs were detected in the liver and spleen and <1% of total injected MNPs were excreted. Additionally, the exposure to an alternating magnetic field and the induction of apoptosis did not affect MNP accumulation. Consequently, localized magnetic heating therapy of tumors might be applied periodically for better therapeutic outcome [19].

## Behavior of MNPs internalized in tumor cells

Using intratumoral injection, MNPs are infiltrated in the tumor region and will bind to the components of the extracellular matrix and/or the cell surface (own unpublished observations). This binding behavior is of electrostatic nature and is influenced by the constitution of the surface coating. If one allows the MNPs to be internalized into cells, e.g. by reasonably extending the time between application and treatment, a higher cell-killing potential is expected because the extracellular heating spots will be transferred to locations inside the cells. In this context, we pre-labeled the cells before implantation as tumor xenograft in mice, measured the temperature at different points, and elucidated the effectivity of treatment *via* histology and biocompatibility *via* blood sample analysis.

From the methodical point of view, BT-474 adenocarcinoma cells were labeled with MNPs (fluidMAG-D, clustered iron oxide cores with diameters of 10 nm and dextran coating; concentration, 0.13 mg Fe/cm<sup>2</sup> growth area; incubation time, 24 h) according to [8]. Severe combined

immune-deficient (SCID) mice were divided into four groups with 5 mice each: group 1, mice with non-labeled BT-474 tumors without magnetic heating; group 2, mice with labeled BT-474 tumors without magnetic heating; group 3, mice with non-labeled BT-474 tumors with magnetic heating; group 4, mice with labeled BT-474 tumors with magnetic heating. Experiments were started when tumor volumes reached approximately 200 mm<sup>3</sup>. For magnetic heating of tumors, mice were exposed to an alternating magnetic field (frequency, 400 kHz; magnetic field strength, 24.6 kA/m) for 300 s. Rectal and intratumoral (central, dorsal, ventral) temperatures were monitored during magnetic heating *via* thermocouples. Mice were sacrificed by CO<sub>2</sub> 2 h after tumor treatment. Subsequently, the blood and internal organs, such as spleen, liver, lung, etc., were extracted for iron analysis *via* atomic absorption spectrometry. Non-treated animals served as control for normal iron in the blood. All experiments were approved by the regional animal care committee and were in accordance with international guidelines on the ethical use of animals.

The treatment of animals resulted in a significant ( $p < 0.03$ , univariate variance analysis) increase in temperatures in the tumor containing labeled cells compared with non-labeled ones. Furthermore, temperatures in tumors of mice with MNPs rose significantly ( $p < 0.02$ ) compared with the corresponding rectal temperatures (see Figure 2).

Interestingly, no distinct differences in blood parameters among the animal groups were detected (Table 1).

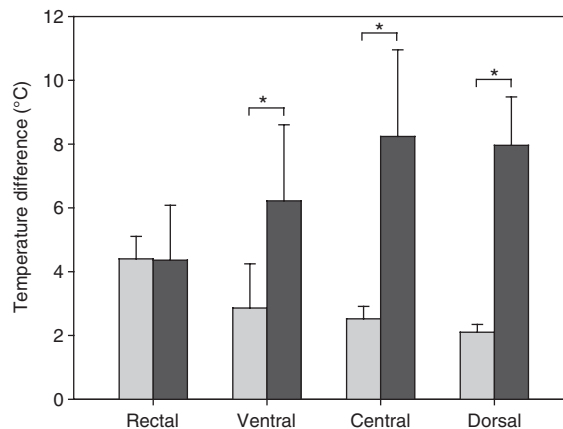


**Figure 2:** Temperature increases during magnetic heating of adenocarcinoma (BT-474) xenografts in mice.

Xenografts consisted of labeled tumor cells. Exposure time: 300 s in an alternating magnetic field (frequency  $f=400$  kHz, amplitude  $H=24.6$  kA/m). Temperature differences with respect to the situation before starting the heating procedure. \*Significantly different with  $p \leq 0.05$ . Light bars: tumors with MNPs, dark bars: tumors without MNPs. Mean and standard deviation of  $n=5$ .

**Table 1:** Hemograms of mice after magnetic heating of BT-474 breast adenocarcinomas.

	I	II	III	IV
<b>Differential hemograms</b>				
Iron (mg Fe/l)	392±128	418±130	445±28	460±123
Erythrocytes (10 <sup>12</sup> /l)	9.3±0.8	10.0±0.8	10.3±1.3	10.7±0.2
Hemoglobin (mmol/l)	8.3±0.2	9.2±0.9	9.2±0.8	9.5±0.2
Hematocrit (%)	39.0±1.5	41.5±5.2	42.1±3.1	41.4±1.6
Leucocytes (10 <sup>9</sup> /l)	1.3±1.0	3.1±3.3	2.4±1.7	1.8±1.1
Lymphocytes (%)	74.9±5.1	72.8±16.1	72.9±20.7	83.9±8.6
Monocytes (%)	14.9±4.1	3.5±1.8	13.4±1.6	9.4±10.1
Neutrophilic granulocytes (%)	6.6±5.8	0.9±0.8	0.6±0.6	0.9±0.8
Eosinophilic granulocytes (%)	0.0±0.0	0.4±0.5	0.3±0.3	0.1±0.2
Basophilic granulocytes (%)	5.1±2.9	22.6±15.6	12.8±22.1	6.3±4.1
Thrombocytes (10 <sup>9</sup> /l)	632.0±384.5	792.7±479.2	1188.0±135.9	1109.6±268.6
<b>Sera</b>				
Creatinines (μmol/l)	28.0±6.2	30.7±7.2	24.4±0.9	22.0±4.0
γ-Glutamyltransferases (μmol/s)	<0.07	<0.07	<0.07	<0.07
Glutamate dehydrogenases (μmol/s)	549.5±171.8	836.5±17.7	773.7±480.7	832.3±425.7
Lactate dehydrogenases (μmol/s)	14.1±8.1	26.9±7.6	18.3±7.4	14.6±4.2
Total bilirubin (μmol/l)	<1.7	<1.7	≤1.7	<1.7
Direct bilirubin (μmol/l)	<1.8	4.2	<1.8	<1.8

I, mice without MNPs or MWF; II, without MNPs and with MWF; III, with MNPs but without MWF; IV, with MNPs and MWF. Mean and standard deviation of n=5.

This is an indication that magnetic heating of fully labeled tumor cells is highly biocompatible. Also, the blood iron contents remained constant in all animal groups and no increase of iron was found in the organs (Figure 3). Therefore, magnetic heating of labeled tumor cells does not induce a systemic delivery of MNP at least at 2 h after treatment.

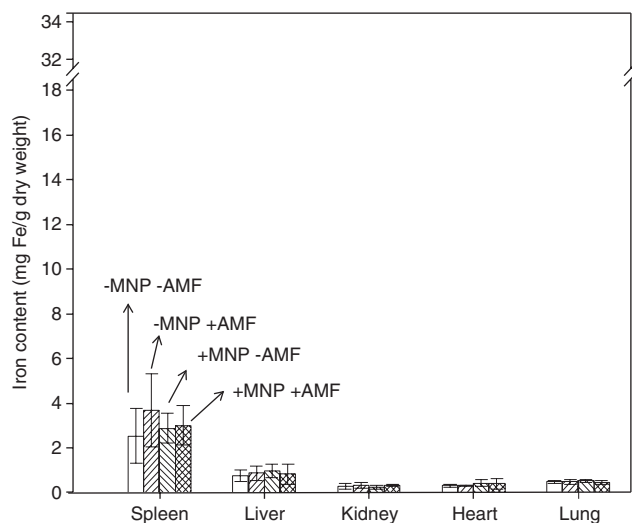


**Figure 3:** Magnetic hyperthermia of labeled cells does not induce a systemic release of iron into the organism. Iron oxide content of different organs of BT-474 tumor-bearing SCID mice. Mean and standard deviation of n=5.

Labeled cells that have been implanted as xenografts in mice and that finally formed a tumor tissue were macroscopically dark after histological processing (Figure 4). This observation indicates that internalized MNPs have not been degraded during tumor growth times of 77±32 days, independently of the heating procedure. Therefore, MNPs internalized into tumor cells are able to remain for a long period. Rather, nanoparticle “dilution” could potentially occur as a result of cell division. Accordingly, the organs (heart, liver, lung, kidney, spleen) of the different mice groups revealed no significant differences in their iron contents with respect to the controls.

All tumors were histologically categorized to belong to the group “G-3” of ductal breast cancer. This means that the used BT-474 tumor xenograft is a highly malignant, low-differentiated tumor with metastatic potential, prominent nuclear polymorphism, and tubuli formation. Treated labeled tumor cells exhibited the highest proportion of necrotic tissue in comparison to the other groups (semi-quantitative scoring: +0.5, +0.6, and +1.0; see Table 2, Figure 4). In labeled cells, no differentiation between cytoplasm and cell nuclei was possible. In the other animal groups (controls for MNPs, the magnetic field, the therapeutic outcome), only very small areas of avital tumor tissue were detected. All tumor samples revealed signs of desmoplasia and hyalinosis (Figure 4).

In conclusion, it seems favorable to modulate the intratumoral application in such a way that MNPs are

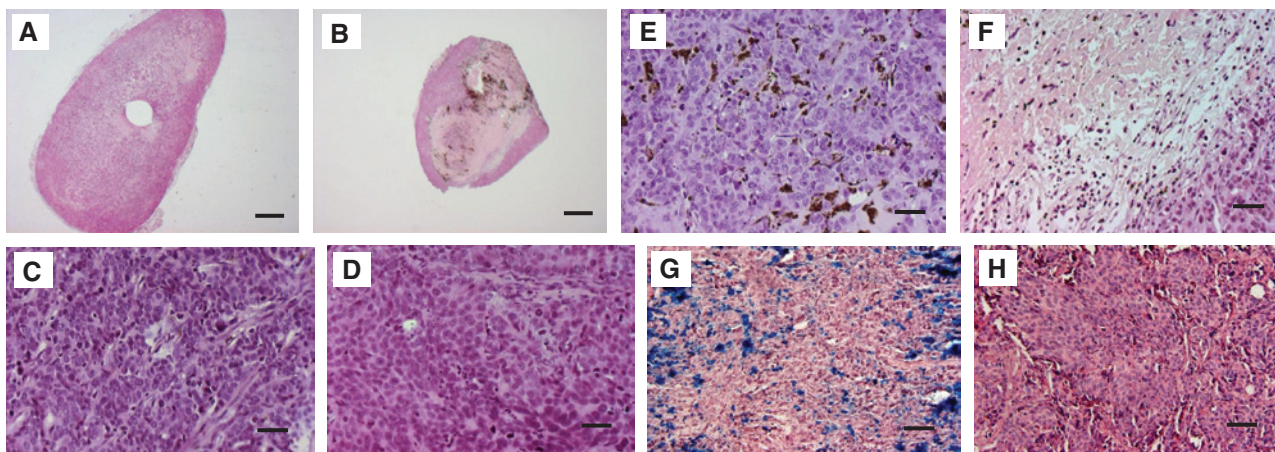


**Figure 4:** Effects of magnetic heating of adenocarcinoma (BT-474) xenografts in mice after magnetic labeling of tumor cells.

(A) No MNPs (-MNPs) no exposure to an alternating magnetic field (-AMF, parameters), bar: 500  $\mu$ m; (B) +MNPs, +AMF, bar: 500  $\mu$ m; (C) +MNPs, -AMF bar: 50  $\mu$ m; (D) -MNPs, +AMF, bar: 50  $\mu$ m; (E) +MNPs, -AMF, bar: 50  $\mu$ m; (F) +MNPs, +AMF, bar: 50  $\mu$ m; (G) -MNPs, -AMF, bar: 50  $\mu$ m; (H) +MNPs, -AMF, bar: 50  $\mu$ m. (A–F) Hematoxylin and eosin staining and (G–H) Prussian blue.

**Table 2:** Histological analysis of tumor sample xenograft in SCID mice and stained with hematoxylin and eosin.

	Grading	Brown pigmentation and hemosiderin	Necrosis	Avital tumor tissue	Desmoplasia and hyalinosis
+MNPs, +AMF	G-3	+1.4	+2.4	0	+1.0
+MNPs, -AMF	G-3	+1.2	+0.6	+0.2	+1.0
-MNPs, +AMF	G-3	0	+1.0	+0.8	+1.0
-MNPs, -AMF	G-3	0	+0.5	0	+1.0

Semiquantitative scoring of features defined in the table (0, not present, to 3, highly pronounced). The malignancy was graded by the degree of de-differentiation (grading, G1 to G3).

internalized into the target cells. This strategy offers the advantage of induction of intracellular heat spots, which increases the therapeutic efficacy as well as the possibility of multiple therapeutic sessions because the MNPs remain in the cells for a long period.

## Design of MNPs as multifunctional tools for magnetic hyperthermia in combination with chemotherapy

The behavior of MNPs internalized into cells has an implication for the utilization of MNPs that have been functionalized with chemotherapeutic agents. The combination of both localized chemotherapy and localized magnetic heating based on the simultaneous use of MNPs as drug carriers and as therapeutic agents is rare. From the combination strategy, advantage can be taken from the already observed additive effect of hyperthermia in combination with chemotherapy, in comparison to respective single treatments [14, 37]. Few examples reported up to now represent

the design of cisplatin- [2, 21] or doxorubicin- [28, 29] loaded MNPs. Apart from that, the largest number of studies are dealing with drugs coupled to MNPs exclusively for magnetic drug targeting purposes. In this context, most studies refer to mitoxantrone (e.g. [1]) or doxorubicin (e.g. [34]) as chemotherapeutic agent.

Cisplatin is one of the most potent antitumor agents in a wide variety of solid tumors. It interacts with DNA to form DNA adducts, primarily intra-strand cross-link adducts, which activate several signal transduction pathways, including ATR protein kinase (Ataxia telangiectasia and Rad3 related), p53, p73, and mitogen activated protein kinase (MAPK), leading to apoptosis activation [31]. We showed that cisplatin can be adsorbed to MNPs by simple incubation (e.g.  $13.4 \pm 2.2$  mg cisplatin/g Fe). In the presence of water and using hyperthermal (42°C) or thermal ablative (60°C) temperatures, cisplatin did not desorb from the MNPs. Nevertheless, when exposed to salts (buffer) or serum albumin, cisplatin was released from the MNPs to a degree of 50% and 25% of the total amount of adsorbed molecules. The facilitated desorption of cisplatin from the MNPs in biological media implicates

its primary utilization for intratumoral deposition of the magnetic material because exposure to blood would result in premature desorption of this chemotherapeutic agent before accumulating at the tumor region due to of the presence of serum albumin [21].

Another alternative is the design of multimodal MNP probe based on the chemotherapeutic agent mitomycin C (MMC). MMC also shows additive toxic effects when combined with heating treatments [37] and is already being used in clinical breast cancer therapy. Studies synthesizing MMC prodrugs reported the covalent binding of MMC to polymers using the cross-linker carbodiimide to connect amino-carboxyl groups. In this context, Kojima et al. [22] conjugated MMC through a carbodiimide-catalyzed reaction onto activated cationic charged dextran. They postulated that a 1 mg conjugate was estimated to contain ~100 µg MMC as determined from spectrophotometric analysis. A few years later, the same group developed a MMC-dextran conjugate with anionic charge again using the carbodiimide coupling procedure [35]. Hereto, the coupling efficiency was similar to the first study, using ~8% (w/w) MMC with respect to the whole MMC-dextran conjugate. Apart from dextran as conjugation partner, Song et al. [32] coupled MMC with *N*-succinyl-chitosan or carboxymethyl-chitin (carbodiimide method) to get a macromolecular prodrug for avoiding the undesirable side effects of MMC after systemic application. An MMC binding of ~120 µg MMC/mg *N*-succinyl-chitosan and carboxymethyl-chitin, respectively, could be achieved, as measured with spectrophotometric methods. Although these coupling efficiencies with non-nanoparticle-associated polymers are very promising, it should be kept in mind that the reactive groups (-OH, -COOH, etc.) of those polymers also react with the magnetite/maghemite cores of MNPs, forming stable shells [23, 27]. Consequently, comparatively fewer free reactive groups are supposed to be available when coupling a chemotherapeutic drug to

an MNP as compared to simple polymer coupling on free polymer molecules. Therefore, a lower coupling efficiency for MMC-MNPs is likely to occur. In addition, MMC is unstable at both acidic [39] and alkaline [3] pH. Therefore, it is imperative to determine the change in drug concentration (drug degradation) during the synthesis procedure and in *in vitro* and *in vivo* experiments. These aspects have not been sufficiently considered by some groups up to now.

To assess a potential degradation of MMC during coupling reactions, it is important to (1) perform degradation measurements on the pH-sensitive MMC with each coupling procedure and (2) time-, pH-, and media-dependent stability measurements on MMC should be carried out to previous coupling investigations.

To distinguish a covalent coupling from an unspecific adsorptive binding, a comparative experimental approach in the absence of the respective cross-linker (1-ethyl-3-(3-dimethylaminopropyl)carbodiimide (EDC) or glutardialdehyde) is beneficial along with each coupling procedure (control of adsorptive binding). Furthermore, an equimolar MMC solution could serve as control for degradation of pH-sensitive MMC during experimentation (control of MMC stability). The MMC concentration bound to carboxymethyl-dextran (CMD) and MNPs can be determined indirectly by measuring unbound MMC in the supernatant and the washing solutions using spectrophotometric and analytical HPLC methods. MMC determinations in the supernatants instead of direct determinations of MMC coupled to MNPs are necessary due to the high absorption properties and consequently the pronounced signal overlay of MNPs on the MMC signal as shown *via* spectrophotometric experiments (own unpublished results). In this context, covalent coupling is only indicated when MMC amounts in supernatants were lower than in the absence of the cross-linker (control of adsorptive binding) and the control of MMC stability (see Table 3). In contrast, adsorptive binding can be expected, when MMC concentrations

**Table 3:** Hypothetical example of MMC determinations in the supernatants after coupling or adsorptive binding reactions toward iron oxide MNPs (here, 5 mg) in the presence or absence of a cross-linker.

	Adsorptive binding of MMC toward MNPs (mg MMC/ml)	Covalent coupling of MMC toward MNPs (mg MMC/ml)
Control of MMC stability	6	6
MMC coupling approach to MNPs without cross-linker (Control of adsorptive binding)	4	5.5 (<6)
MMC coupling approach to MNPs with cross-linker	$4 \leq x < 6$	4 (<5.5)

Here, MMC is stable with 6 mg/ml (control of MMC stability). The exemplary calculation of an adsorptive binding revealed a MMC binding toward MNPs of 2 mg MMC/5 mg MNPs (control of MMC stability minus control of adsorptive binding). The exemplary calculation of a covalent coupling of MMC toward MNPs showed that 1.5 mg MMC/5 mg MNPs had covalently coupled and that additionally 0.5 mg MMC/5 mg MNPs was adsorptively bound.

in supernatants with cross-linker were similar or higher in comparison to supernatants without cross-linker, but still lower than the MMC stability control.

MMC can be coupled to nanoparticles functionalized with arachidonic acid (e.g. fluidMAG-ARA) using the carbodiimide method. Carbodiimides (here, EDC) represent a binary covalent binding system. They are known to react with carboxyl groups of MNPs to give highly reactive *O*-acylisourea derivatives, which themselves react readily with amino groups of the ligand (here, MMC). To couple MMC to the carboxyl groups of fluidMAG-ARA, the carbodiimide method *via* the one-step (without removing EDC) or the two-step (removing EDC) coupling procedure can be performed. In this context, it is important to adapt the concentrations of reactants, solvents buffers, pH values, and incubation times (Table 4). Besides the coupling procedures using EDC alone, EDC together with *N*-hydroxysulfosuccinimide sodium salt (sulfo-NHS) as cross-linker can be added. Sulfo-NHS is known to enhance the coupling efficiency by preparing amine-reactive esters of carboxylate groups (stabilizes the unstable ester *O*-acylisourea [12]) for chemical labeling with primary amines of MMC molecules to form amide cross-links (Figure 5) at neutral pH values [in 0.1 M phosphate buffered saline (PBS) buffer, pH 7.4]. Complementing the approaches with carbodiimide, the utilization of covalent coupling reactions glutardialdehyde as cross-linker is another potential strategy (Table 5, Figure 5). We observed that the best stability of MMC was achieved for the composite solvent ddH<sub>2</sub>O/methanol (2:1; pH 7.0). A similar situation was found for hyperthermal temperatures of 43°C within the therapeutic period of 0.5 h. No MMC was lost at pH 5.0 after 2 h of incubation, representing the relevant period for coupling procedures, whereas 30% degraded within 24 h. In contrast, a rapid degradation of MMC was observed in ddH<sub>2</sub>O, pH 5.0. At longer incubation periods of 24 h in ddH<sub>2</sub>O, pH 5.0, only 10% of the included MMC remained stable.

The highest covalent coupling efficiency was 14.4 µg MMC/mg fluidMAG-ARA using the one-step method. Without consideration of controls for adsorptive binding

(reactions without EDC: 9 µg MMC/mg fluidMAG-ARA binding efficiency), a covalent coupling efficiency (reactions in presence of EDC) of 23.4 µg MMC/mg fluidMAG-ARA instead of 14.4 µg MMC/mg fluidMAG-ARA would have been supposed (Table 6).

Our own studies showed that the covalent coupling of MMC to non-nanoparticle-associated CMD (MMC-CMD) and the analysis of the coupling products MMC-CMD yielded an apparent covalent MMC coupling to CMD of 9.5 µg MMC/mg CMD. Nevertheless, also in the sample without the cross-linker EDC (control of adsorptive binding), we found a concentration of 9.8 µg MMC/mg CMD. Furthermore, a loss of 3.6 µg MMC, in comparison to initial MMC amounts, was detected in the control of MMC stability (equimolar mass of MMC in 0.1 M 2-(*N*-morpholino)ethanesulfonic acid sodium salt (MES) buffer, pH 5.0, without CMD or EDC), representing MMC degradation during the coupling procedure. Consequently, an adsorptive binding of 6.2 µg MMC/mg CMD can be postulated, but no covalent coupling. In contrast, when considering approaches for covalent coupling (MMC in the presence of EDC and CMD), without the aforementioned controls for adsorptive binding and MMC degradation, a covalent coupling of 9.5 µg MMC/mg CMD would have been expected (Table 6).

In own investigations, the most promising coupling parameters were found in relation to the one-step method with 20 mg fluidMAG-PEI, 30% glutardialdehyde (w/v), and 2 mg MMC/ml ddH<sub>2</sub>O and methanol (2:1, pH 7.5) incubated for 16 h. After subtracting the degraded MMC amount as determined from the MMC stability control together with the MMC adsorptively bound to fluidMAG-PEI, a covalent coupling of ~32.4 µg MMC/mg fluidMAG-PEI could be calculated (Table 6). This result could be confirmed using six reproducibility measurements. In contrast, considering a MMC stability control with equimolar masses of glutardialdehyde, 0 µg MMC/mg MNP was obtained (see Table 7). Obviously, spectrophotometric or HPLC analysis were enormously challenging in presence of glutardialdehyde, which means that the coupling

**Table 4:** Experimental conditions during the covalent coupling procedures of the amino groups of MMC to the carboxyl groups of fluidMAG-ARA (5 mg; shell: polymeric ARA) by the carbodiimide method using EDC as cross-linker.

Method					EDC		MMC	
	c (mg/ml)	Solvent	pH	t (min)	c (mg/ml)	Solvent	pH	t (h)
One-step	4.5	0.1 M MES	5.0	–	0.4	0.1 M MES	5.0	0.45
Two-step	22–73	0.1 M MES	5.0, 6.5	10–240	0.1–6.1	ddH <sub>2</sub> O/methanol or 0.1 M MES buffer	5.5	2–14

Listed are EDC and MMC concentrations added to the different solvents at defined pH values over diverse incubation times during a one-step (without removing EDC) or two-step (removing EDC) step coupling procedure.

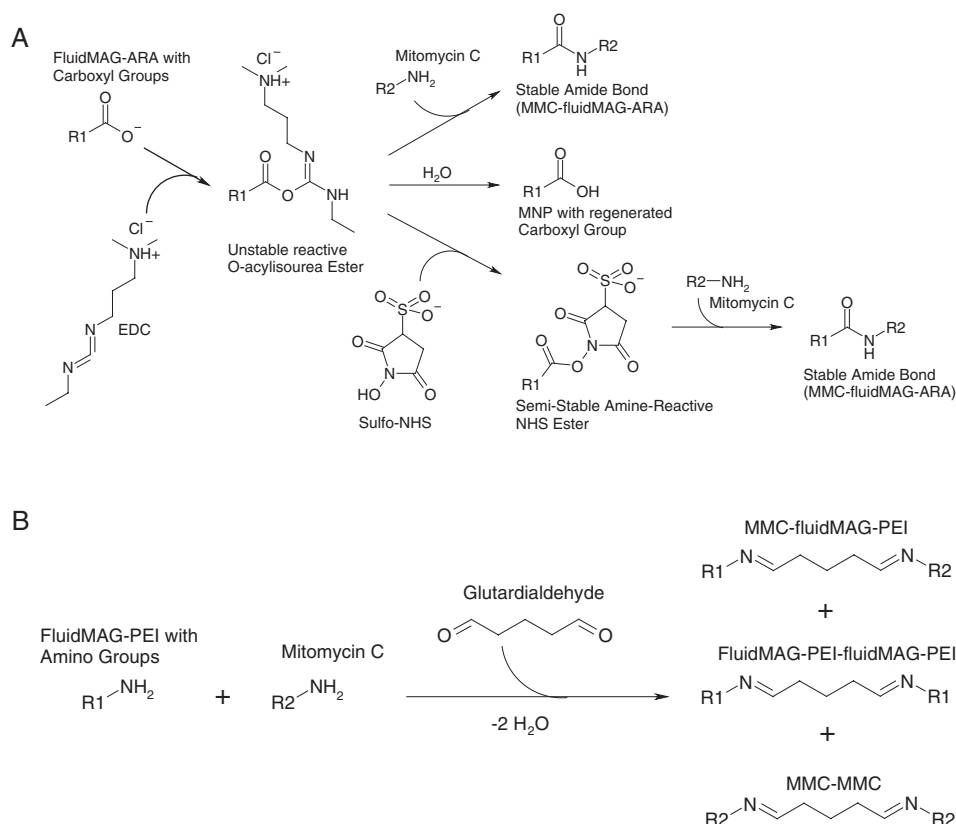


**Figure 5:** Design of multifunctionalized MNPs for magnetic hyperthermia and chemotherapy with MMC.

(A) Reactions of fluidMAG-ARA after activation with the cross-linker EDC, including the activation of MNPs as an NHS ester for covalent coupling of MMC (modified from Thermo Scientific, Pierce Biotechnology user manual for NHS and sulfo-NHS reactions). (B) Reactions of fluidMAG-PEI and MMC after activation with the cross-linker glutaraldehyde. The side product “MMC-MMC” was separated from the product MMC-fluidMAG-PEI and the second side product fluidMAG-PEI-fluidMAG-PEI during the washing procedures. MMC-fluidMAG-PEI and fluidMAG-PEI-fluidMAG-PEI cannot be separated from each other during the protocols used in this study. Scheme used with permission from Thermo Fisher Scientific, copyright 2015.

**Table 5:** Experimental conditions during the covalent coupling procedures of the amino groups of MMC to the amino groups of fluidMAG-PEI (5 mg; shell: polyethylenimine) by the glutaraldehyde (cross-linker) method.

Method	Glutaraldehyde		MMC	
	c (%)	t (h)	c (mg/ml)	t (h)
One-step	1.4–27.8	0	1.9–2.6	1.4–16
Two-step	15	3	3.3–6.7	14

Listed are glutaraldehyde and MMC concentrations in 33.3% methanol (pH 7.5) over diverse incubation times during a one-step (without removing the cross-linker) or two-step (removing the cross-linker) step coupling procedure.

reagent might support MMC degradation or impair accurate measurements.

Within the current investigations, we were able to covalently couple  $\sim 15 \mu\text{g}$  MMC/mg fluidMAG-ARA using the carbodiimide method and around twice as much onto

**Table 6:** Covalent coupling efficiencies of MMC toward iron oxide MNPs or CMD as determined by the use of appropriate controls together with corresponding estimations without controls.

	$\mu\text{g}$ MMC bound/ mg MNP or CMD determined with appropriate controls	$\mu\text{g}$ MMC bound/ mg MNP or CMD estimated without controls
FluidMAG-ARA	14.4	23.4
Free CMD	0.0	9.5
FluidMAG-PEI	32.4	32.4

For further details, see text.

fluidMAG-PEI using the glutaraldehyde method. Owing to the consideration of appropriate controls (control for adsorptive binding and MMC stability) and dedicated experimental conditions, a chemical binding of MMC toward MNPs took place. In contrast, past studies dealing

**Table 7:** Significance of appropriate controls during the estimation of coupled MMC to MNPs (here, fluidMAG-PEI, or PEI) using the glutardialdehyde method.

MMC content ( $\mu\text{g}$ )/mg PEI <sup>a</sup>		Corresponding MMC content ( $\mu\text{g}$ ) without PEI <sup>b</sup>	
MMC+GA	MMC-GA	MMC stability control-GA	MMC stability control+GA
23.7 $\pm$ 9.1	0 $\pm$ 4.5	0 $\pm$ 3.2	23.1 $\pm$ 7.9

Glutardialdehyde (GA) method: 100  $\mu\text{g}$  MMC was added to 1 mg PEI in the presence of GA (30% of the cross-linker) in 33.3% methanol (pH 7.5) incubated >16 h during a one-step coupling procedure (without removing the cross-linker). MMC concentrations that are supposed to be covalently coupled per mg PEI (MMC+GA) are listed together with the MMC concentrations adsorptively bound per mg PEI (MMC-GA). The MMC amount is the amount that was degraded both after the incubation (MMC stability control-GA) and in the presence of GA after incubation (MMC stability control+GA). Mean and standard deviation from six coupling procedures.

<sup>a</sup>Measured indirectly; <sup>b</sup>Measured directly (for further details see text).

with the binding of MMC toward polymers did not perform the necessary controls. We were able to show that suitable controls are essential to study MMC stability and the occurrence of adsorptive binding of MMC toward the polymeric reaction partner to substantiate the coupling efficiencies of MMC to the respective polymer. Therefore, on the basis of the evidence presented in this investigation, it can be concluded that we were able to covalently bind MMC to MNPs with the help of correct controls for MMC stability and adsorptive binding.

## Impact of magnetic heating of cells and tissues

With regard to the impact of magnetic heating, former studies revealed that it modifies the normal structure of phospholipids, proteins, and nucleic acids. Ultimately, the integrity of cellular structures deteriorates [6, 7]. Nevertheless, only little has been known concerning the protein expression of anti-apoptotic B-cell lymphoma 2 (BCL2), fibroblast growth factor receptor 1 (FGF-R1; plays an important role in promotion of tumor growth, differentiation, survival, and angiogenesis), and heat shock protein (HSP70; protein chaperon and modulator of protein folding) after short-time magnetic thermoablative tumor treatment. In our recent study, immunohistochemical analysis of tumor tissue slices revealed a distinct downregulation of BCL2 and FGF-R1 on the protein level, whereas the HSP70 level remained

unchanged. At the same time, tumor tissue exhibited large apoptotic and necrotic areas in regions with high MNP concentration [33].

Importantly, multidrug resistance-associated proteins (MRPs) are known to be responsible for many therapeutic failures in current oncological treatments. The combination of different effectors such as hyperthermia, iron oxide MNPs, and chemotherapeutics is able to downregulate the presence of MRP-1 and MRP-3 at the cell surface, as revealed for an adenocarcinoma cell line. The different MRP-1 and MRP-3 expression levels were not associated with *de novo* mRNA expression, but rather with an altered translocation of MRP-1 and MRP-3 to the cell membrane as a result of reactive oxygen species production and with shifting of intracellular MRP storage pools, changes in membrane fluidity, etc. at the protein level. These results could be used to develop new treatment strategies by repressing mechanisms that actively export drugs from the target cell, thereby improving the therapeutic outcome in oncology [11].

## Challenges of accumulation of the magnetic material at the tumor area through intravenous application

In general, the accumulation of MNPs *via* injection into the veins might be an alternative to intratumoral infiltration, in particular in terms of facilitating a homogeneous distribution throughout the vital and vascularized area of the tumor. This is because tumor vessels differ from normal ones in relation to their shape, defectiveness (poor alignment of endothelial cells etc.), and leakiness. The lack of a lymphatic system in tumors is additionally expected to improve nanoparticle retention in tumors. To facilitate their extravasation from the vascular system into the tumor interstitium, MNPs should be smaller than 200 and 400 nm [26], a requirement that counteracts with the specifications for MNPs with higher heating potential [25].

Another important feature deals in the recognition of MNPs by macrophages as a result of adsorption of immunoglobulins, albumin, and components of the complement system. For this reason, most of the intravenously injected MNPs are taken up by the mononuclear phagocyte system (MPS; formerly designated as reticulo-endothelial system) before having the opportunity to reach the tumor site. Accordingly, in most cases, <3% of the injected dose will ultimately reach the tumor site [16]. In this context, people have tried to use polyethylene glycol (PEG) to

reduce recognition *via* the MPS and prolong the blood circulation time.

Using magnetorelaxometry, we could show that the presence of serum albumin (e.g. in the blood) induces nanoparticle aggregation and that its strength depends crucially on the type of coating. Therefore, the observed aggregation behavior was related to the mechanism of agglutination of MNPs by serum compartments, for example IgG. Interestingly, no aggregation was induced for MNPs coated with dextran, polymeric ARA, or sodium phosphate, respectively [30].

To analyze the potential to use PEG-coated MNPs with a sufficient absorption rate for intravenous application and their enrichment at the tumor site *via* the tumor vascularization, we investigated the biodistribution of amino-PEGylated MNPs and their preferential sites of accumulation in SCID Balb/c mice carrying T24 bladder tumors between the hind legs. After intravenous injection (250–500  $\mu\text{g}$  Fe/animal), we analyzed the nanoparticle distribution at two different points in time by magnetic particle spectroscopy. Moreover, the opsonization of MNPs after their application *in vivo* was investigated by pre-incubating MNPs in mouse serum. Afterward, the impact of opsonization on the biodistribution was analyzed. A special targeting magnet ( $B_0$ , 0.64 T at the surface; gradient, 10 T/m) for an increased enrichment of MNPs in

the tumor was sought to facilitate intratumoral nanoparticle accumulation.

We found that amino-PEGylated MNPs ( $D_H=164$  nm and negative  $\zeta$  potential, both in water) enrich mostly in liver (41% of the injected dose) and lungs (16% of the injected dose) at 1 h after application. Interestingly, 1% of the MNPs accumulated in the lungs after 24 h of application. Unexpectedly, no tumoral MNP accumulation even *via* magnetic targeting could be detected (24 h after injection). This means that the recognition of MNPs *via* the MPS was still too fast to give the MNPs a chance to approach the tumor and get attracted by the magnet.

Pre-incubation of amino-PEGylated MNPs in serum ( $D_H=50$  nm in water and  $>1$   $\mu\text{m}$  in serum;  $\zeta$  potential, positive in water and negative in serum) displaces the preferential accumulation from lungs to the liver. Accordingly, no nanoparticle pre-incubation in serum leads to accumulation in the lungs (also macroscopically visible) (Figure 6).

Taken together, it is challenging to modulate the accumulation of magnetic material by their injection into the vessel system. Hereto, the amounts accessing the tumor tissue are distinctly controlled by pharmacodynamics laws. In this context, more research should be undertaken to unveil dedicated strategies on how to better modulate the pharmacodynamics of MNPs. More details on this topic can be extracted from [16]. One strategy is

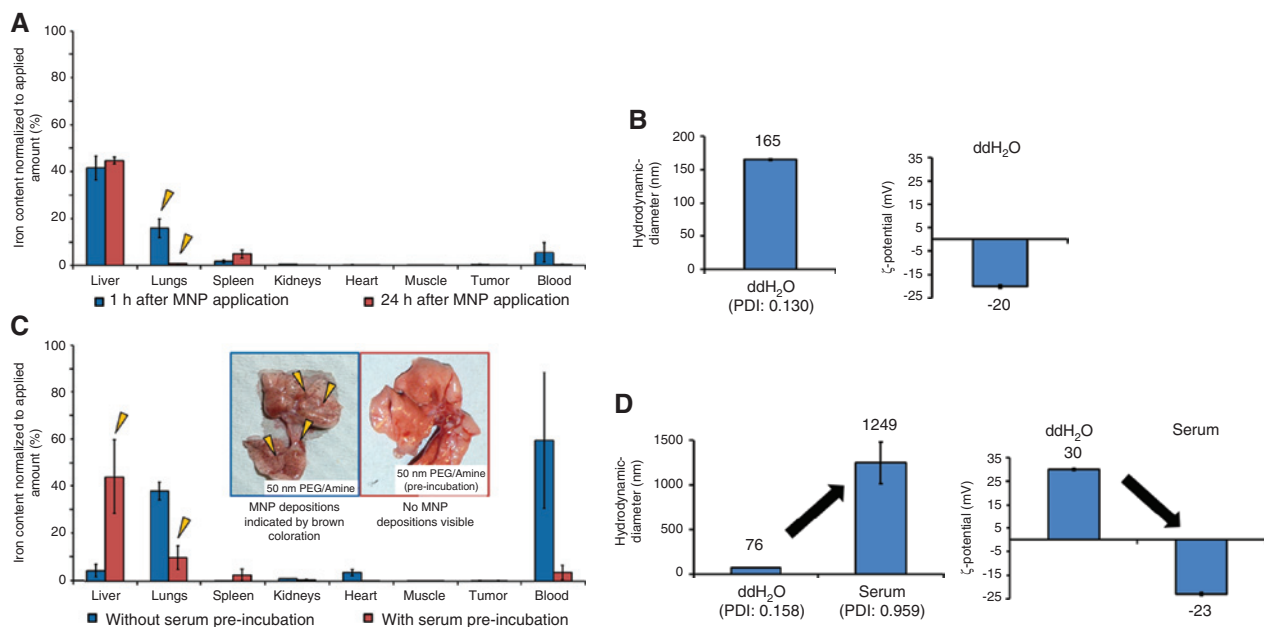


**Figure 6:** Intravenously applied MNPs were cleared from the bloodstream primarily by liver and lungs possibly through the MPS, and pre-incubation in serum influences biodistribution.

(A) Biodistribution after intravenous application, (B) Hydrodynamic diameter of amino-PEGylated MNPs in water. (C) Biodistribution after intravenous application, (D) Hydrodynamic diameter of amino-PEGylated MNPs in water before and after incubation in mouse serum.

Administration of 18 g Fe/kg body weight. Mean and standard deviation of  $\geq 2$ .

the utilization of external magnetic field gradients to concentrate the amount of magnetic materials in the tumor before being cleared by the monocyte phagocyte system. In this context, a high accumulation of chemotherapeutic drugs (e.g. mitoxantrone) previously bound to nanoparticles could be achieved [36].

## Conclusion

In conclusion, there are several means to increase the therapeutic efficiency of magnetic hyperthermia: (1) by distinctly assessing the heating potential of immobilized MNPs and not purely in water as has been done in the past; (2) the intratumoral distribution pattern might well be modulated by specific nanoparticle coating and magnetic targeting; (3) by imaging nanoparticle depositions to correct the distribution *via* multiple applications; (4) by performing multiple therapeutic sessions, as MNPs are not delivered from the tumor site during the heating process; (5) by the utilization of MNPs that internalize into cells to induce intracellular heating spots rather than extracellular ones; (6) utilization of MNPs functionalized with chemotherapeutic agents to favor the additive effects of both therapeutic modalities. We have observed dedicated cytopathological and histopathological alterations in tumors due to hyperthermia after intratumoral application of the magnetic material. Nevertheless, their accumulation at the tumor *via* intravenous application remains a challenge.

**Acknowledgments:** This work was supported by the German Research Foundation (DFG) under contract number HI 698/7. We gratefully acknowledge Stephanie Gräbner for doing experimentation on MMC coupling to MNPs as well technical contribution of Susann Burgold, Julia Göring, and Stephanie Kynast. We also thank Dr. Kurt Gitter for providing a magnet for magnetic targeting experiments and acknowledge Chemicell GmbH (Berlin) and Micromod GmbH (Rostock) for providing the magnetic nanoparticle material. This work is dedicated to Prof. Dr. Werner A. Kaiser, who passed away in December 2013.

**Competing interest:** The authors do not have any personal or financial relationships to disclosure in relation to this article. I.H. holds patents on iron oxide formulations (DE 10 2006 041 495) and on the equipment for induction of magnetic fields (Az 10 2005 062 746.3).

**Authors' contributions:** M.K. wrote the text related to the conjugation of MNPs with MMC and the behavior of MNPs in tumor cells; I.G. did experiments related to the behavior

of MNPs in tumor cells; N.P. investigated the intratumoral distribution of MNPs; M.S. analyzed the biodistribution of MNPs after intravenous application; M.G. did histopathology analysis; U.T. revised the manuscript; I.H. designed, revised, and partially wrote the manuscript.

**Funding:** Deutsche Forschungsgemeinschaft, (Grant/Award Number: HI-698/7).

## References

- [1] Alexiou C, Schmid RJ, Jurgons R, et al. Targeting cancer cells: magnetic nanoparticles as drug carriers. *Eur Biophys J* 2006; 35: 446–450.
- [2] Babincová M, Altanerová V, Altaner C, Bergemann C, Babinec P. In vitro analysis of cisplatin functionalized magnetic nanoparticles in combined cancer chemotherapy and electromagnetic hyperthermia. *IEEE Trans Nanobiosci* 2008; 7: 15–19.
- [3] Beijnen JH, den Hartigh J, Underberg WJ. Quantitative aspects of the degradation of mitomycin C in alkaline solution. *J Pharm Biomed Anal* 1985; 3: 59–69.
- [4] Berkov D. Basic physical principles. In: Andrä WN, Nowak H, editors. *Magnetism in medicine, a handbook*. Berlin: Wiley-VCH Verlag 2007: 26–64.
- [5] Cervadoro A, Cho MJ, Key J, et al. Synthesis of multifunctional magnetic nanoflakes for magnetic resonance imaging, hyperthermia, and targeting. *ACS Appl Mater Interfaces* 2014; 6: 12939–12946.
- [6] Dewey WC. Arrhenius relationships from the molecule and cell to the clinic. *Int J Hyperthermia* 1994; 10: 457–483.
- [7] Dikomey E, Franzke J. Effect of heat on induction and repair of DNA strand breaks in X-irradiated Cho cells. *Int J Radiat Biol* 1992; 61: 221–233.
- [8] Domey J, Haslauer L, Grau I, Strobel C, Kettering M, Hilger I. Probing the cytotoxicity of nanoparticles: experimental pitfalls and artifacts. In: Wegener J, editor. *Bioanalytical reviews*. Volume 3. Heidelberg: Springer 2015. DOI: 10.1007/11663\_2013\_8.
- [9] Dutz S, Kettering M, Hilger I, Müller R, Zeisberger M. Magnetic multicore nanoparticles for hyperthermia – influence of particle immobilization in tumour tissue on magnetic properties. *Nanotechnology* 2011; 22: 265102.
- [10] Eberbeck D, Kettering M, Bergemann C, Zirpel P, Hilger I, Trahms L. Quantification of the aggregation of magnetic nanoparticles with different polymeric coatings in cell culture medium. *J Phys D* 2010; 43: 405002.
- [11] Franke K, Kettering M, Lange K, Kaiser WA, Hilger I. The exposure of cancer cells to hyperthermia, iron oxide nanoparticles, and mitomycin C influences membrane multidrug resistance protein expression levels. *Int J Nanomed* 2013; 8: 351–363.
- [12] Grabarek Z, Gergely J. Zero-length crosslinking procedure with the use of active esters. *Anal Biochem* 1990; 185: 131–135.
- [13] Gupta AK, Gupta M. Synthesis and surface engineering of iron oxide nanoparticles for biomedical applications. *Biomaterials* 2005; 26: 3995–4021.
- [14] Herman TS, Henle KJ, Nagle WA, Moss AJ, Monson TP. Effect of step-down heating on the cyto-toxicity of adriamycin,

- bleomycin, and cis-diamminedichloroplatinum. *Cancer Res* 1984; 44: 1823–1826.
- [15] Hildebrandt B, Wust P, Ahlers O, et al. The cellular and molecular basis of hyperthermia. *Crit Rev Oncol Hematol* 2002; 43: 33–56.
- [16] Hilger I, Kaiser WA. Iron oxide-based nanostructures for MRI and magnetic hyperthermia. *Nanomedicine* 2012; 7: 1443–1459.
- [17] Hilger I, Hergt R, Kaiser WA. Towards breast cancer treatment by magnetic heating. *J Magn Magn Mater* 2005; 293: 314–319.
- [18] Hilger I, Hiergeist R, Hergt R, Winnefeld K, Schubert H, Kaiser WA. Thermal ablation of tumors using magnetic nanoparticles – an in vivo feasibility study. *Invest Radiol* 2002; 37: 580–586.
- [19] Kettering M, Richter H, Wiekhorst F, et al. Minimal-invasive magnetic heating of tumors does not alter intra-tumoral nanoparticle accumulation, allowing for repeated therapy sessions: an in vivo study in mice. *Nanotechnology* 2011; 22: 505102.
- [20] Kettering M, Winter J, Zeisberger M, et al. Magnetic nanoparticles as bimodal tools in magnetically induced labelling and magnetic heating of tumour cells: an in vitro study. *Nanotechnology* 2007; 18: 175101.
- [21] Kettering M, Zorn H, Bremer-Streck S, et al. Characterization of iron oxide nanoparticles adsorbed with cisplatin for biomedical applications. *Phys Med Biol* 2009; 54: 5109–5121.
- [22] Kojima T, Hashida M, Muranishi S, Sezaki H. Mitomycin C-dextran conjugate: a novel high molecular weight pro-drug of mitomycin C. *J Pharm Pharmacol* 1980; 32: 30–34.
- [23] Laurent S, Forge D, Port M, et al. Magnetic iron oxide nanoparticles: synthesis, stabilization, vectorization, physicochemical characterizations, and biological applications. *Chem Rev* 2008; 108: 2064–2110.
- [24] Lisy MR, Schuler E, Lehmann F, Czerney P, Kaiser WA, Hilger I. Diagnosis of peritonitis using near-infrared optical imaging of in vivo labeled monocytes-macrophages. *J Biomed Opt* 2006; 11: 064014. DOI: 10.1117/1.2409310.
- [25] Ludwig R, Stapf M, Dutz S, Muller R, Teichgraber U, Hilger I. Structural properties of magnetic nanoparticles determine their heating behavior – an estimation of the in vivo heating potential. *Nanoscale Res Lett* 2014; 9: 602. DOI: 10.1186/1556-276X-9-602.
- [26] Maeda H, Wu J, Sawa T, Matsumura Y, Hori K. Tumor vascular permeability and the EPR effect in macromolecular therapeutics: a review. *J Control Release* 2000; 65: 271–284.
- [27] Masotti A, Pitta A, Ortaggi G, et al. Synthesis and characterization of polyethylenimine-based iron oxide composites as novel contrast agents for MRI. *Magn Reson Mater Phys* 2009; 22: 77–87.
- [28] Pradhan P, Giri J, Rieken F, et al. Targeted temperature sensitive magnetic liposomes for thermo-chemotherapy. *J Control Release* 2010; 142: 108–121.
- [29] Purushotham S, Ramanujan RV. Thermoresponsive magnetic composite nanomaterials for multimodal cancer therapy. *Acta Biomater* 2010; 6: 502–510.
- [30] Richter H, Kettering M, Wiekhorst F, Steinhoff U, Hilger I, Trahms L. Magnetorelaxometry for localization and quantification of magnetic nanoparticles for thermal ablation studies. *Phys Med Biol* 2010; 55: 623–633.
- [31] Siddik ZH. Cisplatin: mode of cytotoxic action and molecular basis of resistance. *Oncogene* 2003; 22: 7265–7279.
- [32] Song Y, Onishi H, Nagai T. Synthesis and drug-release characteristics of the conjugates of mitomycin C with N-succinyl-chitosan and carboxymethyl-chitin. *Chem Pharm Bull (Tokyo)* 1992; 40: 2822–2825.
- [33] Stapf M, Pömpner N, Kettering M, Hilger I. Magnetic thermoablation stimuli alter BCL2 and FGF-R1 but not HSP70 expression profiles in BT474 breast tumors. *Int J Nanomed* 2015; 10: 1931–1939.
- [34] Sun JB, Duan JH, Dai SL, et al. Preparation and anti-tumor efficiency evaluation of doxorubicin-loaded bacterial magnetosomes: magnetic nanoparticles as drug carriers isolated from *Magnetospirillum gryphiswaldense*. *Biotechnol Bioeng* 2008; 101: 1313–1320.
- [35] Takakura Y, Kitajima M, Matsumoto S, Hashida M, Sezaki H. Development of a novel polymeric prodrug of mitomycin C, mitomycin C-dextran conjugate with anionic charge. I. Physicochemical characteristics and in vivo and in vitro antitumor activities. *Int J Pharm* 1987; 37: 135–143.
- [36] Tietze R, Lyer S, Durr S, et al. Efficient drug-delivery using magnetic nanoparticles – biodistribution and therapeutic effects in tumour bearing rabbits. *Nanomed Nanotechnol Biol Med* 2013; 9: 961–971.
- [37] Uchibayashi T, Lee SW, Kunimi K, et al. Studies of effects of anticancer agents in combination with/without hyperthermia on metastasized human bladder cancer cells in chick embryos using the polymerase chain reaction technique. *Cancer Chemother Pharmacol* 1994; 84–87.
- [38] Wust P, Hildebrandt B, Sreenivasa G, et al. Hyperthermia in combined treatment of cancer. *Lancet Oncol* 2002; 3: 487–497.
- [39] Yen WC, Schmittgen T, Au JL. Different pH dependency of mitomycin C activity in monolayer and three-dimensional cultures. *Pharm Res* 1996; 13: 1887–1891.